A physically-based model for strain-induced crystallization in natural rubber. Part I: Life cycle of a crystallite

Alice Gros, Bertrand Huneau, Erwan Verron, Masatoshi Tosaka

A physically-based model for strain-induced crystallization in natural rubber. Part I: life cycle of a crystallite

Alice Gros, Bertrand Huneau, Erwan Verron

Institut de Recherche en Génie Civil et Mécanique (GeM), UMR CNRS 6183, École Centrale de Nantes, BP 92101, Nantes Cedex 3, France

Masatoshi Tosaka

Institute for Chemical Research, Kyoto University, Gokasho, Uji, Kyoto-fu 611-0011, Japan

Abstract

Despite the numerous experimental investigations performed over the past century and more intensively in the last fifteen years, strain-induced crystallization in natural rubber still remains hardly understood in its precise mechanisms: a complete theoretical description for crystallization and melting of the involved crystallites is still needed to derive relevant physically-based mechanical constitutive equations. Therefore, the present Part I of our work proposes a coherent theory describing the full nucleation–growth–melting cycle of these crystallites, by using classical thermodynamics of phase transitions and by accounting for the topological constraints due to the network. A graphical representation of crystallite evolution involving strain, temperature, and crystallite size is then introduced, using a physical parameter to express the change of Gibbs free energy due to surface creation for a unit volume of crystalline phase. Finally, experimental results from literature exhibiting shape-memory effects in rubber are elucidated using this crystallite life cycle theory.

Keywords: cross-linked polymer; crystallization; nucleation; growth; melting; entanglements

1. Introduction

Intensive experimental investigations conducted in the last twenty years on strain-induced crystallization (phase transition taking place during deformation) in natural rubber have provided an expertise of such material responses under various conditions, *e.g.* deformation, temperature and strain rate (Tosaka, 2007; Huneau, 2011; Toki, 2014; Albouy and Sotta, 2015; Candau et al., 2014,

Email address: erwan.verron@ec-nantes.fr (Erwan Verron)

2015a,b,c, 2016). However, the lack of understanding about the mechanisms at the scale of a crystallite inclines model derivations to adopt phenomenological approaches (Kroon, 2010; Mistry and Govindjee, 2014; Guilie et al., 2015). The present Introduction stands for a short overview on how strain-induced crystallization is described at both polymer network and crystallite scales, in order to point out the missing links.

Information on chain orientation and crystalline fraction, measured by X-ray diffraction during deformation, naturally lead authors to propose descriptive models of strain-induced crystallization: deformation induces the orientation of polymer chains, the alignment of which helps crystallite formation. Strain-induced crystallization is thus sometimes compared to flow-induced crystallization, both of them dealing with oriented polymers. In 1947, Flory lays a cornerstone by representing crystallization of a chain (described as a succession of freely-jointed statistical segments) as an alignment of a few consecutive segments in the loading direction. This implies in particular that the remaining amorphous portion of the chain relaxes, as experimentally observed. Considering measurements highlighting a large proportion of amorphous chains remaining un-oriented under deformation, Toki and Hsiao (2003) propose a structure of semi-crystallized network comprised of micro-fibrillar crystallites linked each other by oriented amorphous chains, and surrounded by un-oriented amorphous chains. Tosaka et al. (2004) then suggest, invoking a similar organization of the network, a mechanism of crystallization initiation based on network inhomogeneity, and in which chains having higher local stretch ratios crystallize first. Another model proposed by Tosaka (2009) assumes that the whole network can be represented by a solid elastic and a fluid components in parallel: crystallites form in the elastic network, while chains from the fluid network only progressively stick to them. Fukahori (2010) proposes an opposite two-phase description from experimental considerations: the fluid network (25% of total volume) crystallizes due to the strain prescribed by the vulcanized (elastic) network. Representations by Albouy et al. (2005, 2014), based on Flory's idea of chain relaxation, focus on the evolution of crystallization and melting during deformation: from a given crystallization (or melting) threshold stretch ratio, crystallites progressively form (resp. disappear) in the chain while strain increases (resp. decreases) such that the stretch ratio of the remaining amorphous part remains constant.

However, thresholds and evolution of this phase transition occurring in strained vulcanized polymer networks remain poorly understood, partially because of very small crystallite sizes (*ca* 100 Å) that prevent observations by microscope. In contrast with larger thermally induced crystallites, admitted to be of folded-chain type in spherulites for unstrained films (Andrews, 1962), even the morphology of strain-induced crystallites remains unclear. A bundle-like morphology is supported, more intuitively than experimentally, by the fact that chain orientation induced by deformation would prevent chains to fold (Toki et al., 2002, 2003, 2004). However, it is experimentally observed that amorphous chains are not as oriented as imagined (Toki et al., 2004), making rather possible the existence of such foldings. Crystallite dimensions measured

in chain direction also remain mainly stable while lateral dimensions vary, inclining to favor the existence of foldings which create such characteristic lamellar structures having constant thickness (Candau et al., 2014). The observed rapidity of crystallite formation renders though difficult the diffusion of chains to create foldings (Toki et al., 2002, 2003; Tosaka et al., 2011), and they are also contested by the absence of characteristic patterns of lamellar structures in X-ray (SAXS) investigations (Albouy et al., 2012; Toki et al., 2002; Tosaka et al., 2011). Finally, in a previous work, we also showed that deformation does not solely explain nucleation rate of strain-induced crystallization: the necessity of additionally considering lower values of interface energies (by many orders of magnitude than those of thermal crystallization) indicates that crystallites are more likely to be bundle-like (Gros et al., 2015). Most of the authors propose a mix of the two morphologies, as well as an evolution of morphology upon strain level (Gaylord and Lohse, 1976; Gaylord, 1976; Rault et al., 2006; Nie et al., 2014; Candau et al., 2014) also observable in films of unvulcanized natural rubber (Andrews, 1962, 1964; Shimizu et al., 1998, 2000).

Thus, the following question arises when deriving models: how to predict and include the formation and melting of these small crystallites in constitutive equations? In Flory's crystallization model described above, crystalline portion is assumed to have no folding, and its size is determined such that it satisfies a thermodynamic equilibrium of the semi-crystallite chain (Flory, 1947). This model, as well as its developments (Gaylord and Lohse, 1976; Gaylord, 1976; Smith, 1976), considers one global crystallized portion on a single (or bundle of) chain(s) and does not propose a physical description of crystallite evolution taking into account limited sizes. In spite of that, recent mechanical models adopt it to derive tridimensional constitutive equations of strain-induced crystallization, forcing their approach to remain phenomenological (Kroon, 2011; Mistry and Govindjee, 2014; Guilie et al., 2015; Nateghi et al., 2018; Rastak and Linder, 2018; Khiêm and Itskov, 2018). A better physical description of crystallites is that of Laghmach et al. (2015), who propose a phase field model (considering a continuum field and not chain scales) in which the authors clearly state nucleation, growth and melting theories. Furthermore, Candau et al. (2014) analyze experimental results in the light of the same thermodynamic theories, and propose a new insight on definitions for crystallization and melting thresholds of different populations of crystallites appearing successively. In these works, nucleation and melting of crystallites are described thanks to the classical thermodynamic theory, and growth is assumed to be restricted by topological constraints (presence of crosslinks and entanglements of chains) in the network. This appears all the more justified that restricted chain mobility is a major difference with thermal crystallization, where formed crystallites are larger and entanglements are looser. Indeed, Laghmach et al. consider an accumulation of topological constraints expelled from the newly formed crystalline phase, and, taking into account the associated elastic energy to drive the equilibrium of the system, provide stable final sizes and shapes of a crystallite. Candau et al., also invoking topological constraints, assume that growth stops as soon as crystallites are large enough to be in equilibrium in the amorphous phase. Plagge

and Klüppel (2018) also use this idea in a recent simple physically-based model which we describe further in Part II of this work (Gros et al., 2018) along with its mechanical treatment.

In order to derive tridimensional mechanical models using statistical chains as in Flory's description, a consistent theory similar to that proposed by Laghmach et al. to describe crystallite nucleation, growth and melting is an essential prerequisite, along with a viable definition of crystallization and melting thresholds expressed in terms of stretch ratios as introduced by Candau et al.. Therefore, the present paper proposes such complete and coherent theoretical description of the "nucleation–growth–melting" cycle of strain-induced crystallites, as well as their associated thresholds, to serve as a basis for mechanical models. The theory derived in Section 2 is mainly based on nucleation and melting theories described by Laghmach et al. and Candau et al., combined with a new description of topological constraints in the network in order to account for both thermodynamic aspects and network topology ~~; a similar idea has already been proposed by Plagge and Klüppel (2018)~~. This leads to the derivation of the governing equations of a crystallite life cycle, of which a graphical representation follows. As an illustration, this theory is used in Section 3 to elucidate what triggers crystallite melting in shape-memory behavior of natural rubber (Katzenberg et al., 2011; Heuwers et al., 2012, 2013a,b; Katzenberg and Tiller, 2016). Part II of this work includes the theory to derive the mechanical tridimensional constitutive equations (Gros et al., 2018). Compared to the works of Laghmach et al. (2015), Candau et al. (2014), and Plagge and Klüppel (2018), our theory: (1) depends solely on network characteristics, namely network chain density or equivalently chain length, (2) considers topological constraints as a barrier for not only crystallite growth but also nucleation, for which we propose a derivation which has never been suggested before, and (3) proposes the bases for a standalone crystallization/melting theory which can be included to various mechanical frameworks.

2. Theory

2.1. Crystallization

2.1.1. Motivation for topological conditions

Topological constraints, denoting crosslinks and chain entanglements in the network, act as barriers for crystallites to grow. This is suggested by experimental observations from Trabelsi et al. (2003) indicating that samples pre-stretched at 90°C and let crystallize in the same strained state at −25°C result in final shapes of crystallites following the affine deformation of the network. These shapes keep a constant volume regardless of the stretch ratios, and this volume seems to be related to that available around a crosslink (itself depending on network chain density). Tosaka (2007), mentioning these results, emphasizes the relationship between crystallite sizes and network structure. Finally, Chenal et al. (2007) highlight an optimal network chain density corresponding

to a drastic change in the dependency of both crystallite volume and maximum crystalline degree on network chain density.

Although these results concern final sizes of crystallites (after growth), they are here first applied to nucleation, and then to crystallite growth as Laghmach et al. do. In fact, thermodynamic conditions of crystallization and melting are not sufficient to explain the absence of crystallization in natural rubber at room temperature yet lower than melting temperature, because sizes of *critical nuclei* (nuclei big enough to grow further) can mathematically be calculated for any stretch ratio and even for an unstrained state. This motivates the derivation of another criterion for nucleation, based on the experimental aforementioned evidences: a crystallite can form only if topological constraints let it enough space to do so. Furthermore, from an energetic point of view, a formed crystallite should grow indefinitely and invade the whole amorphous network. Strain-induced crystallites admitting very narrow sizes, a topological limiting condition for growth must be defined in order to set the final sizes of a stable crystallite.

In the following, the classical theory of nucleation in a strained network is first recalled and discussed considering a parallelepipedic crystallite with arbitrary sizes; topological conditions are then taken into account.

2.1.2. Homogeneous nucleation in a strained network

When a nucleus appears from chain fluctuations in a homogeneous amorphous material, its size determines its evolution: the nucleus disappears if it is too small, or grows if it is large enough (Mandelkern, 2002). This size condition can be expressed by the change in Gibbs free energy due to crystallization: melting is favored when the variation is positive, and on the contrary, crystallization is favored if it is negative. This change in Gibbs free energy ΔG for a crystalline nucleus in a material without impurities is

$$\Delta G = A\gamma - V\Delta G_m \tag{1}$$

where A is the area of the interface between the nucleus and the amorphous or melted medium, γ its corresponding interface free energy, V the volume of the crystallite, and ΔG_m the bulk melting free energy per unit volume (the index m denotes melting throughout this paper). These two contributions to ΔG, one unfavorable to crystallization (surface creation represented by $A\gamma$ which is positive) and the other one favorable when $\Delta G_m > 0$ (bulk effects taken into account with $V\Delta G_m$), determine nucleus existence and stability.

A shape of nucleus must be defined in order to specify ΔG. For a nucleus in polymer, interface energies vary depending on the considered surface, *i.e.* parallel or normal to chain direction. Let us consider a parallelepipedic nucleus, whose sizes are $(L_k)_{k\in\{1,2,3\}}$, L_1 being the size in chain direction (referred to as the nucleus or crystallite *thickness*). The assumption $L_2 = L_3$ is often adopted to simplify the reasoning, but since this hypothesis is not verified from experimental results, primary nucleation theory is written here for arbitrary dimensions: L_1, L_2, L_3 are assumed to be independent one to each other.

In such case, the change in Gibbs free energy due to phase transition is

$$\Delta G = 2L_2L_3\gamma_1 + 2L_1L_3\gamma_2 + 2L_1L_2\gamma_3 - L_1L_2L_3\Delta G_m \tag{2}$$

where γ_k are the interface energies corresponding to the interface normal to the direction $k \in \{1,2,3\}$. These energies are usually referred to as *end surface energy* when $k = 1$ and as *lateral surface energy* when $k = \{2,3\}$. The expression of ΔG_m, depending here on the characteristics of the network and not on those of the nucleus, will be specified afterwards. For small strain rates, growth follows when the spontaneous nucleus overcomes an energetic barrier induced by the competition between surface and bulk effects. This barrier is reached for *critical sizes* of nucleus denoted $(L_k^*)_{k\in\{1,2,3\}}$, such that

$$\left.\frac{\partial \Delta G}{\partial L_k}\right|_{L_k=L_k^*} = 0\,, \quad \forall k \in \{1,2,3\}. \tag{3}$$

It results in the following system of equations, for non-zero $(L_k^*)_{k\in\{1,2,3\}}$:

$$\begin{cases} \dfrac{\gamma_1}{L_1^*} + \dfrac{\gamma_2}{L_2^*} = \dfrac{\Delta G_m}{2} \\ \dfrac{\gamma_1}{L_1^*} + \dfrac{\gamma_3}{L_3^*} = \dfrac{\Delta G_m}{2} \\ \dfrac{\gamma_2}{L_2^*} + \dfrac{\gamma_3}{L_3^*} = \dfrac{\Delta G_m}{2} \end{cases} \tag{4}$$

which leads to

$$L_k^* = \frac{4\gamma_k}{\Delta G_m}\,, \quad k \in \{1,2,3\}\,, \tag{5}$$

and to

$$\frac{\gamma_1}{L_1^*} = \frac{\gamma_2}{L_2^*} = \frac{\gamma_3}{L_3^*} = \frac{\Delta G_m}{4}\,. \tag{6}$$

Eq. (6) highlights the proportionality between sizes and corresponding interface energies, stipulated by the Gibbs-Wulff theorem (Wulff, 1901). This also implies that if interface energies are provided, size ratios remain unchanged and equal to interface energy ratios: $\gamma_1 : \gamma_2 : \gamma_3 = L_1^* : L_2^* : L_3^*$ whatever external conditions such as deformation or temperature.

The melting free energy ΔG_m still has to be specified. It represents the difference between the bulk Gibbs free energies of crystalline and amorphous phases per volume unit of crystalline phase, and is defined as follows:

$$\Delta G_m = \Delta H_m - T\Delta S\,, \tag{7}$$

where T is the absolute temperature, and melting enthalpy ΔH_m is assumed to be independent from both chain length and strain. Change in entropy ΔS shall include the effects of crystallization and of deformation, as depicted in Figure 1. Considering the fact that entropy is related to the number of possible configurations of a chain in space, unstrained amorphous state has a higher

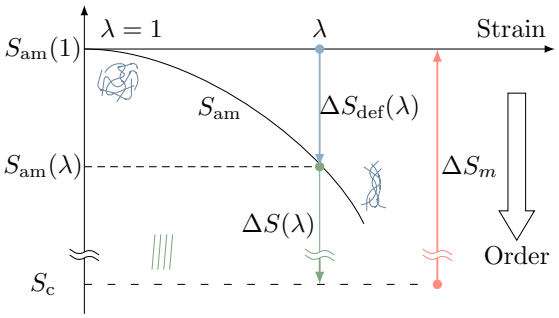

Figure 1: Change in entropy depending on the stretch ratio λ.

entropy $S_{\mathrm{am}}(\lambda = 1)$ than that of crystalline state S_c. Strain induces a decrease in this number of configurations, expressed by a change $\Delta S_{\mathrm{def}}(\lambda) = S_{\mathrm{am}}(\lambda) - S_{\mathrm{am}}(1)$ in entropy, and has a favorable effect towards crystallization. Thus,

$$\Delta G_m = \Delta H_m - T\left(\Delta S_m + \Delta S_{\mathrm{def}}(\lambda)\right) \tag{8}$$

where ΔS_m is the melting entropy of an unstretched material. By definition of the melting temperature of a perfect infinite crystal in an unstrained material T_m^0,

$$\Delta S_m = \frac{\Delta H_m}{T_m^0}\,, \tag{9}$$

and therefore

$$\Delta G_m(\lambda, T) = \left(1 - \frac{T}{T_m^0}\right)\Delta H_m - T\Delta S_{\mathrm{def}}(\lambda) \tag{10}$$

where ΔS_{def} can be expressed from statistical properties of long chain molecules and usually depends on chain length characterized by the number of statistical Kuhn segments (Treloar, 1975). The expression of ΔG_m, incorporated in those of critical sizes (Eq. (5)) finally leads to

$$L_k^* = \frac{4\gamma_k}{\left(1 - \frac{T}{T_m^0}\right)\Delta H_m - T\Delta S_{\mathrm{def}}(\lambda)}\,, \quad k \in \{1,2,3\}\,. \tag{11}$$

It is important to keep in mind that interface energies being positive, these expressions are only defined and physically acceptable when the denominator is strictly positive. Figure 2 shows the influence of stretch ratio on critical sizes for different values of interface energies. The strong influence of γ on L^* emphasizes again how important the values of these interfacial energies are.

Remark 1. *This nucleation theory applies for both folded-chain or bundle-like types of crystallite, and the choice of morphology, including mixed types, is expressed through the values of interface energies (Gros et al., 2015). Besides, their dependency upon deformation and temperature are unknown, and* $(\gamma_k)_{k\in\{1,2,3\}}$ *are assumed to be constant throughout this paper.*

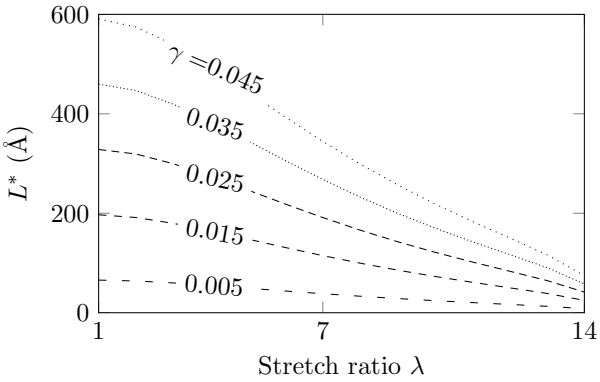

Figure 2: Influence of stretch ratio λ and interfacial energy γ on critical sizes L^* (calculated with $N = 200$, $T = 293$ K). γ varies from 0.005 to 0.035 J/m^3.

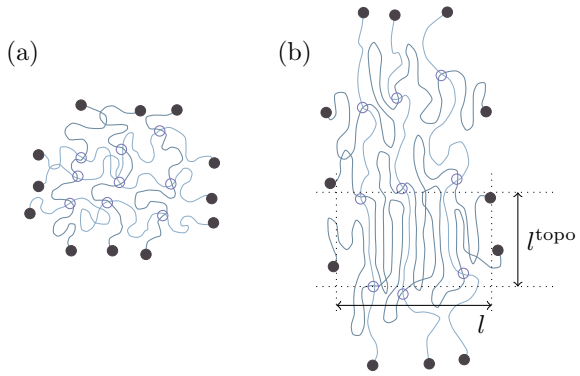

Figure 3: Representation of the network. (a) Undeformed network with crosslinks (filled circles) and entanglements (open circles). (b) Strained network with characteristic lengths l^{topo} and l.

These critical sizes define a so-called *critical nucleus* (smallest nucleus large enough to grow further). In the following, *nucleation* denotes the formation of a crystallite (whose smallest possible size is that of a critical nucleus), and *crystallization* refers to both nucleation and growth.

2.1.3. Crystallization in a network with topological constraints

Figure 3(a) shows an undeformed network with crosslinks (filled circles) and entanglements (open circles). In the proposed conditions of nucleation and growth, these topological constraints prevent nuclei to invade the whole network: as shown in Fig. 3(b) with a strained configuration, entanglements along a chain prevent nuclei to spread all along it, and in the direction normal to the chain, crosslinks play this role. As depicted, entanglements do not constitute barriers in the lateral direction because the crystallite is assumed to be constituted by

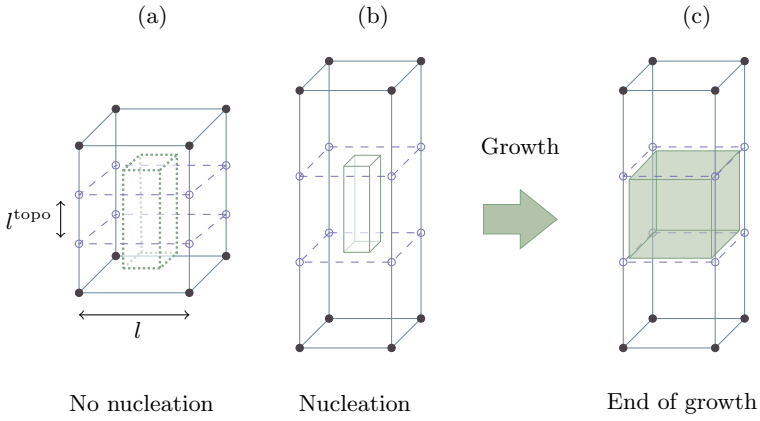

Figure 4: Conditions of crystallization (nucleation and end of growth). (a) The chains of the strained network (solid lines) are punctuated by crosslinks (filled circles) and entanglements (open circles), which dictate nucleation (dotted lines). (b) When the network is further strained, the thickness of the critical nucleus is smaller than the length between two entanglements and nucleation occurs, defining crystallization threshold. (c) Instantaneous lateral growth follows until reaching a stable size.

different chains aligned in the deformation direction. The space allowed by these topological constraints is assimilated to a parallelepiped, whose characteristic lengths are the distance between two consecutive entanglements along a chain (denoted l^{topo}) in chain direction, and that between two crosslinks (denoted l) in the lateral directions. Entanglements are assumed to follow the deformation of the chain it belongs to, and the network can thus be seen as a tessellation of space by parallelepipeds.

For a given stretch ratio λ, the thickness L_1^* of a critical nucleus can be calculated with Eq. (11), as well as the distance l^{topo} between two entanglements. The present condition assumes that nucleation occurs only if the thickness of the critical nucleus is smaller than the length between two entanglements:

$$L_1^*(\lambda) \leqslant l^{\text{topo}}(\lambda)\,. \tag{12}$$

as depicted in Figures 4(a) and (b), where chains (solid line) join crosslinks (filled circles) with each other and are impeded by entanglements (open circles).

- In state (a), where the network is lightly strained, the thickness of the critical nucleus (symbolized as a dotted parallelepiped) is larger than the length between two entanglements and nucleation does not occur.

- When the network is further strained (Fig. 4(b)), the length between two entanglements increases compared to state (a) and the thickness of the critical nucleus decreases (see Fig. 2). Nucleation occurs when these two lengths become equal.

Since L_1^* decreases with λ while l^{topo} increases with it, the threshold stretch ratio of crystallization λ_c is

$$\lambda_c = \arg\min_{\lambda>0} \left[L_1^*(\lambda) - l^{\text{topo}}(\lambda) \right] . \tag{13}$$

Growth is then assumed to be instantaneous after nucleation (Albouy et al., 2012; Brüning et al., 2012; Candau et al., 2012; Tosaka et al., 2012), and such reached maximal sizes (denoted $(\breve{L}_k)_{k\in\{1,2,3\}}$) to be kept afterwards. The thickness of the crystallite, still limited by the entanglements, does not change ($\breve{L}_1 = L_1^*$). In lateral directions, growth is assumed to be limited by crosslinks, as represented in Figure 4(c). Invoking the incompressibility of the network, the distance between two crosslinks in the lateral direction is the end-to-end distance l of a chain stretched at $1/\sqrt{\lambda_c}$. Thus, the final sizes $(\breve{L}_k)_{k\in\{1,2,3\}}$ of the crystallite are finally

$$\breve{L}_k = \begin{cases} l^{\text{topo}}(\lambda_c) & \text{for} \quad k = 1 \,, \\ l\left(\frac{1}{\sqrt{\lambda_c}}\right) & \text{for} \quad k \in \{2,3\} \,. \end{cases} \tag{14}$$

2.2. Melting

Melting conditions of the previous crystallite are now investigated. They simply derive from classical thermodynamic equations and do not introduce new definition, condition, nor hypothesis.

2.2.1. Definition of the melting point

The change in Gibbs free energy due to the melting of the crystallite (of sizes $(\breve{L}_k)_{k\in\{1,2,3\}}$) can be written as follows:

$$\Delta G = 2\breve{L}_2\breve{L}_3\gamma_1 + 2\breve{L}_1\breve{L}_3\gamma_2 + 2\breve{L}_1\breve{L}_2\gamma_3 - \breve{L}_1\breve{L}_2\breve{L}_3\Delta G_m(\lambda, T) \tag{15}$$

where $\Delta G_m(\lambda, T)$ is given by Eq. (10). Despite the similarity of Eqs. (2) and (15), the unknowns are here λ and T, not the sizes which are defined by Eq. (14). The melting point is characterized by $\Delta G = 0$, such that

$$\sum_{k=1}^{3} \frac{2\gamma_k}{\breve{L}_k} - \Delta G_m(\lambda, T) = 0 \,. \tag{16}$$

Crystallite sizes being known, the melting point is defined by the couple (λ, T) that satisfies Eq. (16).

2.2.2. Two particular cases and deformation-temperature equivalence

Two particular cases of Eq. (16), also discussed in Laghmach et al. (2015) and Candau et al. (2015c), are considered. In the case T is known and constant (not necessarily equal to the temperature at which crystallization took place), melting stretch ratio λ_m satisfies

$$\sum_{k=1}^{3} \frac{2\gamma_k}{\breve{L}_k} - \Delta G_m(\lambda_m, T) = 0 \,. \tag{17}$$

When T is equal to the temperature at which crystallization took place, this describes the usual situation of strain-induced crystallization. λ_m is defined by solving Eq. (17) given an expression for ΔS_{def}.

In the case where λ is known and constant, melting temperature T_m satisfies

$$\sum_{k=1}^{3} \frac{2\gamma_k}{\breve{L}_k} - \Delta G_m(\lambda, T_m) = 0\,. \tag{18}$$

This corresponds to the thermal melting of a crystallite in a deformed network. In Eq. (18), T_m is the melting temperature of a crystallite of dimensions $(\breve{L})_{k\in\{1,2,3\}}$ in a network strained at a given stretch ratio λ, which again can be different from that of crystallization λ_c. Eq. (18) gives

$$T_m = T_m^0 \left(1 - \frac{\sum \frac{2\gamma_k}{\breve{L}_k}}{\Delta H_m}\right)\left(1 + \frac{T_m^0 \Delta S_{\text{def}}(\lambda)}{\Delta H_m}\right)^{-1} \tag{19}$$

and T_m depends on $(\breve{L})_{k\in\{1,2,3\}}$ and λ.

Remark 2. *Given that γ_1 is usually of the same order of magnitude as γ_2 and γ_3, when lateral sizes are large compared to the crystallite thickness,* e.g. *lamellar structures, Eq.* (19) *leads, for an unstrained polymer, to the Gibbs-Thomson relationship (Mandelkern, 2002). Besides, melting temperature for a crystallite with infinite dimensions is also easily retrieved.*

Considering the two aforementioned particular cases for a crystallite formed at the stretch ratio λ_c and the temperature T_c, either a couple (λ_m, T_c) or a couple (λ_c, T_m) satisfying the equilibrium can be determined (Eqs. (17) and (18) resp.). Furthermore, an infinity of couples (λ, T) mathematically satisfy Eq. (16) for each given $(\breve{L})_{k\in\{1,2,3\}}$ in the domains we are interested in (the relationship linking such λ and T is even bijective when $\lambda \geqslant 1$). From a physical point of view, it indicates that for any given temperature, there exists a stretch ratio at which melting point is reached (Miyamoto et al., 2003; Trabelsi et al., 2003; Rault et al., 2006; Candau et al., 2015c), and vice-versa: temperature and deformation are equivalently able to trigger the melting of a crystallite, as introduced by Miyamoto et al. in particular.

2.3. Graphical representation of the crystallite life cycle

The previous derivations highlight the importance of λ, T and crystallite size in describing nucleation, growth and melting. Hence, this section aims to provide a geometric representation of the path followed by a crystallite during its life cycle by using these variables. The description and figures here suppose that there is no temperature change due to the exothermicity of crystallization, that chain relaxation induced by nucleation and growth does not affect the stretch ratio, and that there is no kinetic and diffusion aspects (melting is instantaneous). The previous theory where the stable crystallite is limited by topological constraints in an uniaxial deformation is considered, but the graphical representation holds for more general cases, *e.g.* no topological constraints, additional lateral deformation.

For non-zero $(L_k)_{k\in\{1,2,3\}}$, Eq. (2) can be written

$$\Delta G = L_1 L_2 L_3 \left[\sum_{k=1}^{3} \frac{2\gamma_k}{L_k} - \Delta G_m(\lambda, T) \right] \tag{20}$$

where $\Delta G_m(\lambda, T)$ is specified by Eq. (10). The volume $L_1 L_2 L_3$ of the crystallite being always positive, the term between brackets provides the sign of ΔG. Its second term ΔG_m depends on λ and T, and not on crystallite sizes, which are included instead in the first term, denoted g:

$$g := \sum_{k=1}^{3} \frac{2\gamma_k}{L_k} \,. \tag{21}$$

This term is an indicator of how large crystallites are: low values of g (resp. large values) correspond to large (resp. small) sizes of crystallites. It will thus be used to represent crystallite size, and ΔG is considered as a function of the 3-uple (λ, T, g). From a thermodynamical point of view, g can be interpreted as a change in Gibbs free energy induced by surface creation/disappearance for a unit volume of crystalline phase, in opposition to ΔG_m which is related to bulk effects. The "density" aspect is emphasized when g is expressed as follows:

$$g = \frac{1}{L_1 L_2 L_3} (2L_2 L_3 \gamma_1 + 2L_1 L_3 \gamma_2 + 2L_1 L_2 \gamma_3) \,. \tag{22}$$

From the previous section, there exists an infinity of 3-uples (λ, T, g) at which ΔG vanishes (Eq. (16)), *i.e.* satisfying

$$g - \Delta G_m(\lambda, T) = 0 \,. \tag{23}$$

In a spatial representation, this equation defines a surface, plotted in Figure 5 and denoted $\mathscr{S}$, which can also be interpreted as couples of (λ, T) satisfying Eq. (23) for a given value of g. The intersection of the surface with the plane $g = 0$ (dashed line on the figure) corresponds to the case of an infinite crystallite, and that with the plan $\lambda = 1$ (dotted line in the figure) is the usual case encountered in classical thermal crystallization of an unstrained material. From its definition, this surface $\mathscr{S}$ is comprised of the equilibrium points between amorphous and crystalline phases, and separates the space into two parts: the one "above" (larger values of g at a given (λ, T)) corresponds to $\Delta G(\lambda, T, g) > 0$ (stability of the amorphous phase), and the one "below" (lower values of g) corresponds to $\Delta G(\lambda, T, g) < 0$ (stability of crystalline phase).

Furthermore, crystallite sizes at nucleation and after growth are defined using λ and T thanks to ΔG and topological conditions. It means that although g does not directly depend on λ and T, particular values taken by g depend on λ and T, or, in other words, the state of the crystallite at a given value of g strongly depends on (λ, T), as represented in Figure 6(a) for a given T. When nucleation occurs, from Eq. (6), g takes the value

$$g^* = \sum_{k=1}^{3} \frac{2\gamma_k}{L_k^*(\lambda)} = \frac{3}{2} \Delta G_m(\lambda, T) \,, \tag{24}$$

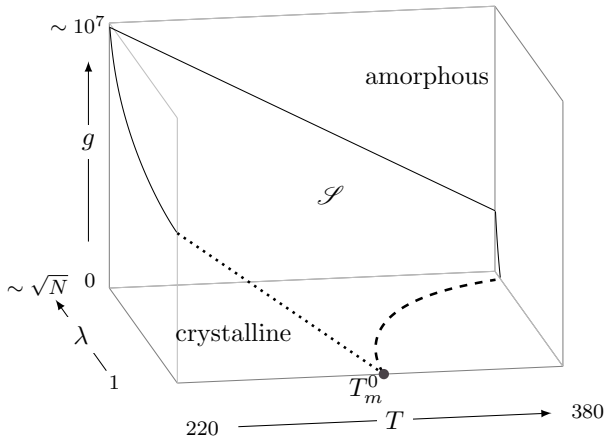

Figure 5: Equilibrium surface of amorphous and crystalline phases. λ ranges from 1 to less than $\sqrt{N}$ (g tends to infinity when λ tends to $\sqrt{N}$). Units: g in J/m^3, T in K, λ without unit.

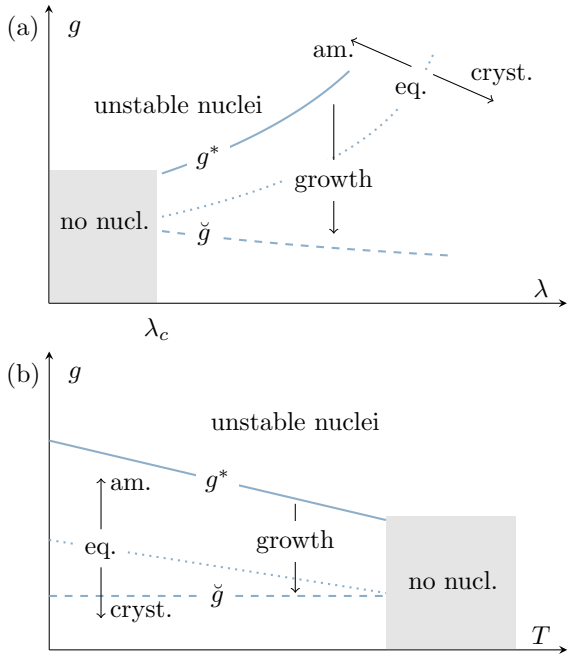

Figure 6: Profiles of Fig. 5: (a) for a given T and (b) for a given λ. Corresponding crystallite states in space depending on (λ, T, g).

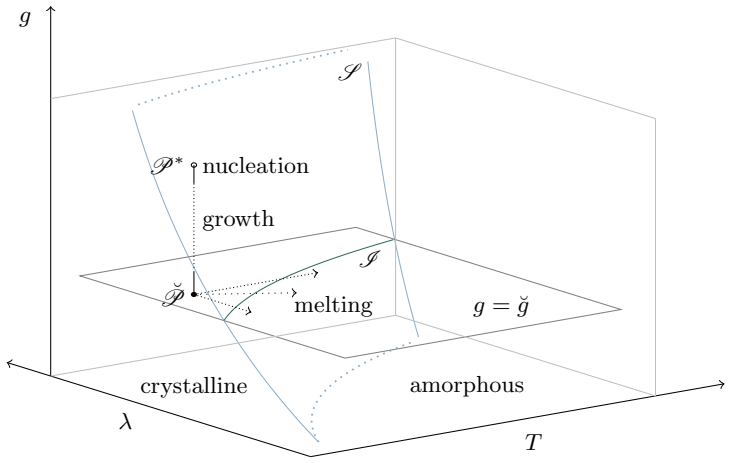

Figure 7: Zoom on a restricted area of Fig. 5 and path of crystallization through the equilibrium surface, from $\mathscr{P}^*$ to $\breve{\mathscr{P}}$. The melting points are along the intersection $\mathscr{I}$ of $\mathscr{S}$ with the plane $g = \breve{g}$.

(solid line). It is situated "above" the equilibrium curve defined by $g = \Delta G_m(\lambda, T)$ (dotted line) which separates crystalline and amorphous domains (Eq. (23)). From the definition of ΔG and its energetic barrier, values of g larger than g^* correspond to unstable nuclei (smaller than the critical sizes). If growth is limited by topological constraints, the lower value reached by g is

$$\breve{g} = \sum_{k=1}^{3} \frac{2\gamma_k}{\breve{L}_k} \tag{25}$$

(dashed line, assuming that λ and T do not vary during the instantaneous growth) where $(\breve{L})_{k\in\{1,2,3\}}$ depend only on the stretch ratio λ_c at which nucleation and growth took place (Eq. (14)). The figure "g vs. T" for a given λ in Fig. 6(b) is similar, except that equilibrium curve and $g = g^*$ curve increase with respect to T, and that the $g = \breve{g}$ curve is a horizontal line according to our topological constraints which do not depend on temperature. In both cases, there exists a domain in which nucleation does not occur if there are topological constraints.

In order to depict the path of (λ, T, g)-uples followed by a crystallite during its life cycle, Figure 7 represents the same surface $\mathscr{S}$ as in Fig. 5 for a smaller domain of T, λ and g. The 3-uple (λ_c, T_c, g^*) corresponding to a crystallite at nucleation defines a point $\mathscr{P}^*$ "above" $\mathscr{S}$. During growth, the 3-uple follows the black line linking $\mathscr{P}^*$ to the point $\breve{\mathscr{P}}$ of coordinates $(\lambda_c, T_c, \breve{g})$ situated "below" $\mathscr{S}$ by crossing it and defined by topological constraints of the network. λ and T are assumed to be constant during growth in Fig. 7.

Once the sizes of the stable crystallite are reached, they do not vary anymore: the 3-uples of the upcoming paths are all restricted to the $(\lambda, T, \breve{g})$-uples

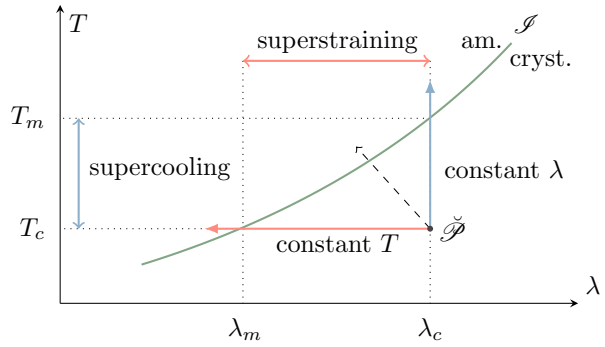

Figure 8: Equilibrium curve $\mathscr{I}$ in the plane $g = \breve{g}$ (intersection with $\mathscr{S}$). Three melting paths from point $\breve{\mathscr{P}}$ (stable crystallite) are depicted: by a change in temperature with λ kept constant (vertical arrow; supercooling effect), by a change in stretch ratio with T kept constant (horizontal arrow, superstraining effect), and another possible path (dashed arrow).

belonging to the plane $g = \breve{g}$. The surface $\mathscr{S}$ being the set of equilibrium points, those belonging to the intersection $\mathscr{I}$ of $\mathscr{S}$ with the plane $g = \breve{g}$, define possible melting points for the crystallite. There exists an infinity of paths leading to melting, consisting in linking $\breve{\mathscr{P}}$ to a melting point belonging to $\mathscr{I}$, as indicated in Fig. 7 by dotted arrows, which cross the melting curve so that the path followed by the melted crystallite reaches the space where amorphous phase is stable. In particular and as depicted in Figure 8, if λ is constant, melting is due to the change in temperature (supercooling effect), and if T is constant, melting is due to deformation (*superstraining* effect as introduced by Candau et al. (2014, 2015c)). Any other path letting both λ and T vary is possible. This figure is similar to that proposed in Chapter 4, Figure C2 in Candau (2014) considering experimental results.

Remark 3. *One can distinguish melting points from equilibrium points for sake of clarity. The equilibrium surface is comprised of the 3-uples satisfying* $\Delta G(\lambda, T, g) = 0$ *and exists prior to any consideration of a specific crystallite. It defines which amorphous phase or crystalline phase is favored under the conditions given by a 3-uple. Melting points, on the contrary, are relative to a specific crystallite and conditions: they are equilibrium points which can be reached given a crystallite size,* i.e. *those belonging to* $\mathscr{I}$*. Furthermore, lowering* T *or increasing* λ *may increase crystallite size: under such assumptions, only the area formed by two arrows (constant* λ *and constant* T*) and* $\mathscr{I}$ a priori *keeps the crystallite as it is, and reachable melting points are restricted to those comprised between* $(\lambda_c, T_m, \breve{g})$ *and* $(\lambda_m, T_c, \breve{g})$ *belonging to* $\mathscr{I}$ *in Fig. 8.*

3. Illustration of the theory

Equivalence of temperature and deformation for triggering melting has already been investigated by Candau et al. (2015c) in the light of experimental results, and a corresponding theory has been derived in the previous section.

The present section therefore emphasizes on how to represent melting conditions as a surface of (λ, T, g)-uples satisfying $\Delta G(\lambda, T, g) = 0$, allows to deal with crystallization and melting analysis with the presence of changes in both temperature and strain.

As a preamble, it is to note that the theory of Section 2 applies to an idealized network comprised of chains having all the same length. A real network, constituted of chains having different lengths (Miyamoto et al., 2003), is here assumed to be comprised of several different idealized networks, and all the chains to deform with the same stretch ratio (Candau et al., 2014). Using such description of the network, this section explicates experimental mechanical response of Heuwers et al. (2013a) of a lightly crosslinked natural rubber undergoing a particular cyclic deformation during which temperature changes. In the following, the experimental procedure and the corresponding results are first described, followed by the life cycle of crystallites under these experimental conditions for a single idealized network and then for the real network.

3.1. Experimental procedure

The experimental step sequence, used by Heuwers et al. (2013a) and making both strain and temperature vary, is depicted in Figure 9(a). Corresponding data of the measured mechanical response (force) are plotted in Figure 9(b) along with points A to H. The different steps are as follows.

1. Loading (A to C): a lightly crosslinked sample of natural rubber is stretched at a given temperature T_s up to a stretch ratio $\lambda_{\max}^{(\exp)}$, whose value depends on crosslinking degree in Ref. 23, and which is assumed to be larger than the macroscopic crystallization threshold. This loading path exhibits a very standard mechanical response: force increases and material stiffens.
2. Cooling and pause (C to D): at $\lambda_{\max}^{(\exp)}$, temperature is decreased from T_s to T_p, and the system remains still during five minutes. In Ref. 23, $T_s = 50°\mathrm{C}$, $T_p = 10°\mathrm{C}$. During these cooling and pausing steps, force significantly decreases.
3. First unload (D to E): unload starts again and is stopped when the decreasing force vanishes, defining a stretch ratio denoted $\lambda_t^{(\exp)}$.
4. Heating (E to F): at $\lambda_t^{(\exp)}$, temperature is then increased back to T_s, triggering a sudden increase in force.
5. Second unload (F to H): unload finally continues until force comes back to zero again.

3.2. Crystallite life cycle

During the loading path A-B-C, experiments usually exhibit a macroscopic threshold stretch ratio at which crystallization starts, followed by successive apparition of crystallites in the network as deformation continues. At the end of the loading path (point C), there are several populations of crystallites having different sizes and belonging to different idealized network (Candau et al., 2014).

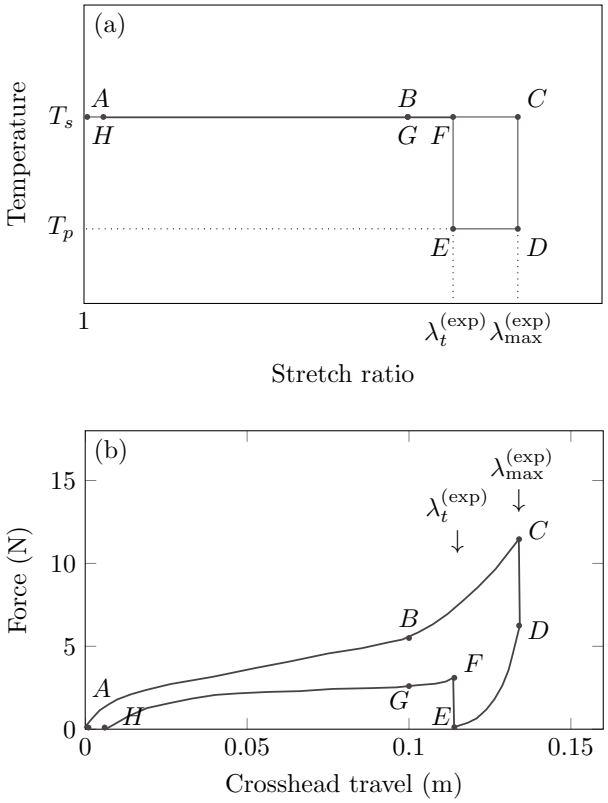

Figure 9: (a) Experimental step sequence and (b) corresponding mechanical response (data extracted from Ref. 23). Points A to H are particular points used in the text.

Let us first consider a single crystallite of given sizes $(\breve{L}_k)_{k\in\{1,2,3\}}$ at point D, formed during the loading path and being larger than at point C due to the growth favored by cooling and chain rearrangement. From the equilibrium surface as in Fig. 5, both strain and temperature decreases induce larger supercooling and superstraining than at T_s. As depicted in Fig. 8, this crystallite can melt because of deformation (steps 3 or 5) or temperature (step 4). Noticing that Figs. 8 and 9(a) admit the same axes, an identical representation is used in Figure 10 to depict these three cases as paths followed during the steps from D to G. $\breve{\mathscr{P}}$ represents the crystallite at point D and $\mathscr{I}$ its melting curve as in Fig. 8. $\lambda_m^{(T_p)}$ and $\lambda_m^{(T_s)}$ denote the threshold stretch ratios of melting of the considered crystallite corresponding to temperatures T_p and T_s respectively.

- Path *D-E-F-G* (solid arrow): if unload stops at a stretch ratio λ_t, first assumed to be larger than $\lambda_m^{(T_p)}$ and smaller than $\lambda_m^{(T_s)}$, and temperature is increased to T_s, it is very likely that the path crosses the equilibrium curve $\mathscr{I}$ (defining point M), meaning that the crystallite melts during

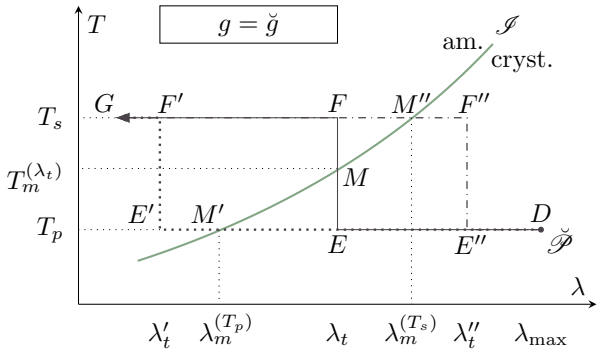

Figure 10: In the plane $g = \breve{g}$, equilibrium curve $\mathscr{I}$ (solid curve), and three cases of paths followed by a crystallite during unload process (D to G): $\lambda_m^{(T_p)} < \lambda_t < \lambda_m^{(T_s)}$ (solid arrow), $\lambda'_t \leqslant \lambda_m^{(T_p)}$ (dotted arrow) and $\lambda''_t \geqslant \lambda_m^{(T_s)}$ (dash-dotted arrow).

this heating process.

- Path D-E'-F'-G (dotted arrow): if unload is stopped at λ'_t such that $\lambda'_t < \lambda_m^{(T_p)}$, the crystallite has already melted (path crossing $\mathscr{I}$ at point M') such as in a standard unload at constant T_p
- Path D-E''-F''-G (dash-dotted arrow): finally, if the path has not crossed yet the equilibrium curve at the end of the heating step, it means that the stretch ratio λ''_t at which unload stops is higher than $\lambda_m^{(T_s)}$ and that the crystallite melts during the following unload process from point F'' to G (path intersecting $\mathscr{I}$ at M'').

The first and third cases are two examples of possible paths previously commented as "letting both λ and T vary" for melting.

These considerations, described for a single population of crystallites in an idealized network, can be generalized to all the crystallites formed in the material, having different sizes and made from chains of different lengths, *i.e.* in different idealized networks. Their corresponding equilibrium curves are different as well and can be represented as a melting area denoted $\{\mathscr{I}\}$, as depicted in Figure 11. Since the intersection of the path of a crystallite with its melting curve means that it melts, the depiction of path crossing the melting area $\{\mathscr{I}\}$ corresponds to a progressive melting of the crystallites in the sample. Let us draw the attention on the fact that this representation is for the whole range $\{\breve{g}\}$ of the $\breve{g}$ calculated from different crystallite sizes in the sample, and not for a given single $\breve{g}$, *i.e.* for a given size of crystallite, as it was the case in Figs. 8 or 10. The starting point is thus denoted $\{\breve{\mathscr{P}}\}$ to indicate that it is not a single point there but a set of them.

Remark 4. *Keeping the prior construction in mind, the mechanical response shown in Fig. 9(b) can be simply described by a descriptive model of the network evolution based on Flory's representation of a semi-crystallized chain.*

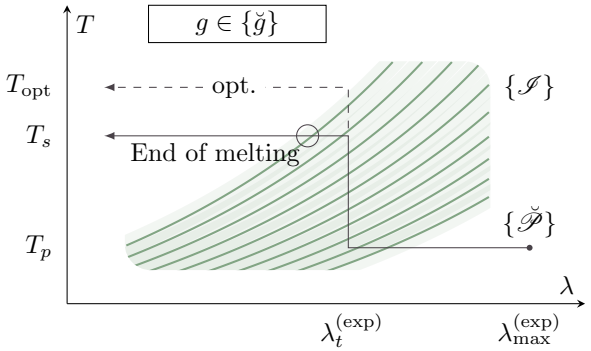

Figure 11: Melting area $\{\mathscr{I}\}$ crossed by the paths of crystallites from different idealized networks constituting the real network during unload (D to H).

Remark 5. *The efficiency of the sample as an energy storage material, emphasized by Heuwers et al., is calculated by the ratio of the area under the curve from F to H (stored energy) to that under the curve from A to C (provided energy) of the mechanical response (Fig. 9(b)). It means that for a given loading process, the higher force the point F reaches, the better the efficiency becomes. Considering the three possible melting paths previously described and the fact that melting leads to an increase of* λ *and of the force, this is equivalent to look for a total melting of the crystallites during the heating process. As shown in Fig. 11, melting of remaining crystallites still continues in the unloading process after the heating step (*$\lambda < \lambda_t^{(exp)}$*), until finishing crossing the meting area (indicated by a circle). To optimize energy storage, temperature should thus be increased up to* T_{opt} *(see Fig. 11), even higher than initial stretching temperature, until all crystallites are melted. This seems all the more interesting that force increases with temperature.*

4. Conclusion

After a brief overview of previous representations of strain-induced crystallization in natural rubber in lieu of an introduction, this paper proposes a consistent theory describing the complete nucleation–growth–melting cycle of crystallites taking into account classical thermodynamic theories and the entangled nature of polymer networks through topological constraints. Its main features are as follows.

- Nucleation treatment follows that of classical homogeneous nucleation, to which a topological condition due to limited chain mobility is added, considering that nucleation cannot take place if entanglements spatially prevent it. Growth, assumed to be instantaneous, is again limited by entanglements, and because of the proposed nucleation condition, only lateral growth is permitted. Melting condition is driven by a standard

consideration of Gibbs free energy, the analysis of which emphasizes an equivalence between temperature and deformation effects.

- A new physical parameter g, related to a change of Gibbs free energy due to surface creation for a unit volume of crystalline phase, is introduced as an indicator of crystallite size.
- The 3-uple (λ, T, g) is used to describe crystallite evolution in a network, and to propose a graphical representation of the crystallite life cycle.

This theory succeeds in describing experimental results on energy storage using shape-memory properties of lightly crosslinked natural rubber, providing bases for further understanding of how to trigger crystallite melting and optimize storage efficiency. Part II of this work (Gros et al., 2018) includes the theory to derive mechanical constitutive equations of a tridimensional model for modeling strain-induced crystallization in natural rubber. It uses the work presented here to govern crystallization and melting evolution in a network having a chain-length distribution, using statistical chains of different lengths.

References

References

Albouy, P.-A., Guillier, G., Petermann, D., Vieyres, A., Sanseau, O., Sotta, P., 2012. A stroboscopic x-ray apparatus for the study of the kinetics of strain-induced crystallization in natural rubber. Polymer 53 (15), 3313–3324.
URL http://dx.doi.org/10.1016/j.polymer.2012.05.042

Albouy, P.-A., Marchal, J., Rault, J., 2005. Chain orientation in natural rubber, part i: The inverse yielding effect. European Physical Journal E 17 (3), 247–259.
URL http://dx.doi.org/10.1140/epje/i2004-10145-6

Albouy, P.-A., Sotta, P., 2015. Strain-Induced Crystallization in Natural Rubber. Advances in polymer science. Springer Berlin Heidelberg, Berlin, Heidelberg, pp. 167–205.
URL http://dx.doi.org/10.1007/12_2015_328

Albouy, P.-A., Vieyres, A., Perez-Aparicio, R., Sanseau, O., Sotta, P., 2014. The impact of strain-induced crystallization on strain during mechanical cycling of cross-linked natural rubber. Polymer 55 (16), 4022–4031.
URL http://dx.doi.org/10.1016/j.polymer.2014.06.034

Andrews, E. H., 1962. Spherulite morphology in thin films of natural rubber. Proceedings of the Royal Society of London A: Mathematical, Physical and Engineering Sciences 270 (1341), 232–241.
URL http://dx.doi.org/10.1098/rspa.1962.0214

Andrews, E. H., 1964. Crystalline morphology in thin films of natural rubber. ii. crystallization under strain. Proceedings of the Royal Society of London A: Mathematical, Physical and Engineering Sciences 277 (1371), 562–570.
URL http://dx.doi.org/10.1098/rspa.1964.0040

Brüning, K., Schneider, K., Roth, S., Heinrich, G., 2012. Kinetics of strain-induced crystallization in natural rubber studied by waxd: Dynamic and impact tensile experiments. Macromolecules 45 (19), 7914–7919.
URL https://doi.org/10.1021/ma3011476

Candau, N., 2014. Compréhension des mécanismes de cristallisation sous tension des élastomères en conditions quasi-statiques et dynamiques. Ph.D. thesis, INSA de Lyon.
URL https://tel.archives-ouvertes.fr/tel-01135298

Candau, N., Chazeau, L., Chenal, J.-M., Gauthier, C., Ferreira, J., Munch, E., Rochas, C., 2012. Characteristic time of strain induced crystallization of crosslinked natural rubber. Polymer 53 (13), 2540–2543.
URL http://dx.doi.org/10.1016/j.polymer.2012.04.027

Candau, N., Chazeau, L., Chenal, J.-M., Gauthier, C., Munch, E., 2015a. Compared abilities of filled and unfilled natural rubbers to crystallize in a large strain rate domain. Composites Science and Technology 108, 9–15.
URL http://dx.doi.org/10.1016/j.compscitech.2014.12.014

Candau, N., Chazeau, L., Chenal, J.-M., Gauthier, C., Munch, E., 2016. Complex dependence on the elastically active chains density of the strain induced crystallization of vulcanized natural rubbers, from low to high strain rate. Polymer 97, 158–166.
URL http://dx.doi.org/10.1016/j.polymer.2016.05.020

Candau, N., Laghmach, R., Chazeau, L., Chenal, J.-M., Gauthier, C., Biben, T., Munch, E., 2014. Strain-induced crystallization of natural rubber and cross-link densities heterogeneities. Macromolecules 47 (16), 5815–5824.
URL http://dx.doi.org/10.1021/ma5006843

Candau, N., Laghmach, R., Chazeau, L., Chenal, J.-M., Gauthier, C., Biben, T., Munch, E., 2015b. Influence of strain rate and temperature on the onset of strain induced crystallization in natural rubber. European Polymer Journal 64, 244–252.
URL http://dx.doi.org/10.1016/j.eurpolymj.2015.01.008

Candau, N., Laghmach, R., Chazeau, L., Chenal, J.-M., Gauthier, C., Biben, T., Munch, E., 2015c. Temperature dependence of strain-induced crystallization in natural rubber: On the presence of different crystallite populations. Polymer 60, 115–124.
URL http://dx.doi.org/10.1016/j.polymer.2015.01.029

Chenal, J.-M., Chazeau, L., Guy, L., Bomal, Y., Gauthier, C., 2007. Molecular weight between physical entanglements in natural rubber: a critical parameter during strain-induced crystallization. Polymer 48 (4), 1042–1046.
URL http://dx.doi.org/10.1016/j.polymer.2006.12.031

Flory, P. J., 1947. Thermodynamics of crystallization in high polymers. 1. crystallization induced by stretching. Journal of Chemical Physics 15 (6), 397–408.
URL http://dx.doi.org/10.1063/1.1746537

Fukahori, Y., 2010. Mechanism of the self-reinforcement of cross-linked nr generated through the strain-induced crystallization. Polymer 51 (7), 1621–1631.
URL http://dx.doi.org/10.1016/j.polymer.2010.01.059

Gaylord, R. J., 1976. Theory of stress-induced crystallization of crosslinked polymeric networks. Journal of Polymer Science Part B: Polymer Physics 14 (10), 1827–1837.
URL http://dx.doi.org/10.1002/pol.1976.180141008

Gaylord, R. J., Lohse, D. J., 1976. Morphological changes during oriented polymer crystallization. Polymer Engineering and Science 16 (3), 163–167.
URL http://dx.doi.org/10.1002/pen.760160308

Gros, A., Huneau, B., Verron, E., Tosaka, M., 2018. A physically-based model for strain-induced crystallization in natural rubber. Part II: derivation of the thermo-mechanical model. Submitted to Journal of the Mechanics and Physics of Solids.

Gros, A., Tosaka, M., Huneau, B., Verron, E., Poompradub, S., Senoo, K., 2015. Dominating factor of strain-induced crystallization in natural rubber. Polymer 76, 230–236.
URL http://dx.doi.org/10.1016/j.polymer.2015.08.058

Guilie, J., Thien-Nga, L., Le Tallec, P., 2015. Micro-sphere model for strain-induced crystallisation and three-dimensional applications. Journal of the Mechanics and Physics of Solids 81, 58–74.
URL http://dx.doi.org/10.1016/j.jmps.2015.05.004

Heuwers, B., Beckel, A., Krieger, A., Katzenberg, F., Tiller, J. C., 2013a. Shape-memory natural rubber: An exceptional material for strain and energy storage. Macromolecular Chemistry and Physics 214 (8), 912–923.
URL http://dx.doi.org/10.1002/macp.201200649

Heuwers, B., Quitmann, D., Hoeher, R., Reinders, F. M., Tiemeyer, S., Sternemann, C., Tolan, M., Katzenberg, F., Tiller, J. C., 2013b. Stress-induced stabilization of crystals in shape memory natural rubber. Macromolecular Rapid Communications 34 (2), 180–184.
URL http://dx.doi.org/10.1002/marc.201200594

Heuwers, B., Quitmann, D., Katzenberg, F., Tiller, J. C., 2012. Stress-induced melting of crystals in natural rubber: a new way to tailor the transition temperature of shape memory polymers. Macromolecular Rapid Communications 33 (18), 1517–1522.
URL http://dx.doi.org/10.1002/marc.201200313

Huneau, B., 2011. Strain-induced crystallization of natural rubber: a review of x-ray diffraction investigations. Rubber Chemistry and Technology 84 (3), 425–452.
URL http://dx.doi.org/10.5254/1.3601131

Katzenberg, F., Heuwers, B., Joerg, J. C., 2011. Superheated rubber for cold storage. Advanced Materials 23, 1909–1911.
URL http://dx.doi.org/10.1002/adma.201100408

Katzenberg, F., Tiller, J. C., 2016. Shape memory natural rubber. Journal of Polymer Science Part B: Polymer Physics 54 (14), 1381–1388.
URL http://dx.doi.org/10.1002/polb.24040

Khiêm, V., Itskov, M., 2018. Analytical network-averaging of the tube model: Strain-induced crystallization in natural rubber. Journal of the Mechanics and Physics of Solids 116, 350 – 369.
URL https://doi.org/10.1016/j.jmps.2018.04.003

Kroon, M., 2010. A constitutive model for strain-crystallising rubber-like materials. Mechanics of Materials 42 (9), 873–885.
URL http://dx.doi.org/10.1016/j.mechmat.2010.07.008

Kroon, M., 2011. An 8-chain model for rubber-like materials accounting for non-affine chain deformations and topological constraints. Journal of Elasticity 102 (2), 99–116.
URL http://dx.doi.org/10.1007/s10659-010-9264-7

Laghmach, R., Candau, N., Chazeau, L., Munch, E., Biben, T., 2015. Phase field modelling of strain induced crystal growth in an elastic matrix. Journal of Chemical Physics 142 (24).
URL http://dx.doi.org/10.1063/1.4923226

Mandelkern, L., 2002. Crystallization of polymers. Volume 1. Equilibrium concepts, 2nd Edition. Cambridge University Press.
URL https://doi.org/10.1017/CBO9780511535413

Mistry, S. J., Govindjee, S., 2014. A micro-mechanically based continuum model for strain-induced crystallization in natural rubber. International Journal of Solids and Structures 51 (2), 530–539.
URL http://dx.doi.org/10.1016/j.ijsolstr.2013.10.027

Miyamoto, Y., Yamao, H., Sekimoto, K., 2003. Crystallization and melting of polyisoprene rubber under uniaxial deformation. Macromolecules 36 (17),

6462–6471.
URL http://dx.doi.org/10.1021/ma0342877

Nateghi, A., Dal, H., Keip, M.-A., Miehe, C., 2018. An affine microsphere approach to modeling strain-induced crystallization in rubbery polymers. Continuum Mechanics and Thermodynamics 30 (3), 485–507.
URL https://doi.org/10.1007/s00161-017-0612-8

Nie, Y., Gao, H., Hu, W., 2014. Variable trends of chain-folding in separate stages of strain-induced crystallization of bulk polymers. Polymer 55 (5), 1267–1272.
URL http://dx.doi.org/10.1016/j.polymer.2014.01.034

Plagge, J., Klüppel, M., 2018. A theory relating crystal size, mechanical response, and degree of crystallization in strained natural rubber. Macromolecules 51 (10), 3711–3721.
URL https://doi.org/10.1021/acs.macromol.8b00177

Rastak, R., Linder, C., 2018. A non-affine micro-macro approach to strain-crystallizing rubber-like materials. Journal of the Mechanics and Physics of Solids 111, 67–99.
URL https://doi.org/10.1016/j.jmps.2017.10.007

Rault, J., Marchal, J., Judeinstein, P., Albouy, P.-A., 2006. Stress-induced crystallization and reinforcement in filled natural rubbers: ^{2}h nmr study. Macromolecules 39 (24), 8356–8368.
URL http://dx.doi.org/10.1021/ma0608424

Shimizu, T., Tosaka, M., Tsuji, M., Kohjiya, S., 2000. Tem observation of natural rubber thin films crystallized under molecular orientation. Rubber Chemistry and Technology 73 (5), 926–936.
URL http://dx.doi.org/10.5254/1.3547630

Shimizu, T., Tsuji, M., Kohjiya, S., 1998. A TEM study on natural rubber thin films crystallized under molecular orientation. Journal of the Society of Materials Science, Japan 47 (2), 117–120.
URL http://dx.doi.org/10.2472/jsms.47.6Appendix_117

Smith, K. J. J., 1976. Crystallization of networks under stress. Polymer Engineering and Science 16 (3), 168–175.
URL http://dx.doi.org/10.1002/pen.760160309

Toki, S., 2014. 5 - the effect of strain-induced crystallization (sic) on the physical properties of natural rubber (nr). In: Kohjiya, S., Ikeda, Y. (Eds.), Chemistry, Manufacture and Applications of Natural Rubber. Woodhead Publishing, pp. 135 – 167.
URL http://dx.doi.org/10.1533/9780857096913.1.135

Toki, S., Hsiao, B. S., 2003. Nature of strain-induced structures in natural and synthetic rubbers under stretching. Macromolecules 36 (16), 5915–5917.
URL http://dx.doi.org/10.1021/ma034729e

Toki, S., Sics, I., Ran, S., Liu, L., Hsiao, B. S., Murakami, S., Tosaka, M., Kohjiya, S., Poompradub, S., Ikeda, Y., Tsou, A. H., 2004. Strain-induced molecular orientation and crystallization in natural and synthetic rubbers under uniaxial deformation by *in-situ* synchrotron x-ray study. Rubber Chemistry and Technology 77 (2), 317–335.
URL http://dx.doi.org/10.5254/1.3547826

Toki, S., Sics, I., Ran, S. F., Liu, L., Hsiao, B. S., Murakami, S., Senoo, K., Kohjiya, S., 2002. New insights into structural development in natural rubber during uniaxial deformation by *in situ* synchrotron x-ray diffraction. Macromolecules 35 (17), 6578–6584.
URL http://dx.doi.org/10.1021/ma0205921

Toki, S., Sics, I., Ran, S. F., Liu, L. Z., Hsiao, B. S., 2003. Molecular orientation and structural development in vulcanized polyisoprene rubbers during uniaxial deformation by *in situ* synchrotron X-ray diffraction. Polymer 44 (19), 6003–6011.
URL http://dx.doi.org/10.1016/S0032-3861(03)00548-2

Tosaka, M., 2007. Strain-induced crystallization of crosslinked natural rubber as revealed by x-ray diffraction using synchrotron radiation. Polymer Journal 39, 1207–1220.
URL http://dx.doi.org/10.1295/polymj.PJ2007059

Tosaka, M., 2009. A route for the thermodynamic description of strain-induced crystallization in sulfur-cured natural rubber. Macromolecules 42 (16), 6166–6174.
URL http://dx.doi.org/10.1021/ma900954c

Tosaka, M., Murakami, S., Poompradub, S., Kohjiya, S., Ikeda, Y., Toki, S., Sics, I., Hsiao, B. S., 2004. Orientation and crystallization of natural rubber network as revealed by waxd using synchrotron radiation. Macromolecules 37 (9), 3299–3309.
URL http://dx.doi.org/10.1021/ma0355608

Tosaka, M., Senoo, K., Sato, K., Noda, M., Ohta, N., 2012. Detection of fast and slow crystallization processes in instantaneously-strained samples of cis-1,4-polyisoprene. Polymer 53 (3), 864–872.
URL http://dx.doi.org/10.1016/j.polymer.2011.12.035

Tosaka, M., Toki, S., Che, J., Rong, L., Hsiao, B. S., 2011. Development of internal fine structure in stretched rubber vulcanizates. Journal of Polymer Science Part B: Polymer Physics 49 (16), 1157–1162.
URL http://dx.doi.org/10.1002/polb.22290

Trabelsi, S., Albouy, P.-A., Rault, J., 2003. Crystallization and melting processes in vulcanized stretched natural rubber. Macromolecules 36 (20), 7624–7639.
URL http://dx.doi.org/10.1021/ma030224c

Treloar, L., 1975. The Physics of Rubber Elasticity. Monographs on the physics and chemistry of materials. Oxford University Press.

Wulff, G., 1901. Zur frage der geschwindigkeit des wachsthums und des auflösung der krystallflächen. Zeitschrift für Krystallographie und Mineralogie 34 (1-6), 449–530.
URL http://dx.doi.org/10.1524/zkri.1901.34.1.449